

Quantitative Experimental Study of Defects Induced by Process Parameters in the High-Pressure Die Cast Process



P. SHARIFI, J. JAMALI, K. SADAYAPPAN, and J.T. WOOD

A quantitative experimental study of the effects of process parameters on the formation of defects during solidification of high-pressure die cast magnesium alloy components is presented. The parameters studied are slow-stage velocity, fast-stage velocity, intensification pressure, and die temperature. The amount of various defects are quantitatively characterized. Multiple runs of the commercial casting simulation package, ProCAST™, are used to model the mold-filling and solidification events. Several locations in the component including knit lines, last-to-fill region, and last-to-solidify region are identified as the critical regions that have a high concentration of defects. The area fractions of total porosity, shrinkage porosity, gas porosity, and externally solidified grains are separately measured. This study shows that the process parameters, fluid flow and local solidification conditions, play major roles in the formation of defects during HPDC process.

<https://doi.org/10.1007/s11661-018-4633-0>

© Her Majesty the Queen in Right of Canada, as represented by the Minister of Natural Resources 2018

I. INTRODUCTION

CONCERNING the emission of greenhouse gasses as well as the reduction of fuel consumption, the automotive industry is driven to seek lightweight solutions in the development of robust components. Magnesium is a good candidate for this purpose due to the excellent strength-to-weight ratio.^[1–5] Many of the complex magnesium components are produced through the high-pressure die casting (HPDC) process, due to its much faster production rate compared with other casting methods, while it is an economic and efficient method for producing components with high-dimensional accuracy. However, the application of die cast magnesium alloys in vehicle structures is limited by variations in the mechanical properties of geometrically complex components.^[2]

The variations in mechanical properties have been found to depend upon casting defects such as gas and shrinkage porosities, defect band, and externally solidified crystals (ESGs).^[6,7] These defects adversely affect the mechanical properties of die cast magnesium alloys,

such as ductility and yield strength.^[6–8] Previous studies reported that the amounts of defects show dependency on the process parameters such as melt temperature, gate velocity, die temperature, intensification pressure, casting geometry, slow stage of piston velocity, and fast stage of piston velocity, and venting gate area.^[8–11] Dargusch *et al.*^[9] investigated the effects of intensification pressure and casting second-stage velocity on the volumetric porosity for complex geometry of die cast aluminum alloys. The authors concluded that the increase in the intensification pressure reduces total volumetric porosity; on the other hand, the increase in the second-stage velocity significantly increases volumetric porosity. Other studies^[8,12,13] confirm that the ductility of aluminum and magnesium alloys depend primarily upon the area fraction of porosity rather than on the volumetric porosity. Thus, volumetric porosity is not a suitable characteristic for studying the effects of process parameters on the defect formation.

Haug *et al.*^[10] studied the effects of intensification pressure, and the first- and the second-stage piston velocities on the total area fraction of porosity for a simple geometry of die cast magnesium alloy. They considered shrinkage and gas porosities together as total area fraction of porosity, while there is a difference in their formation mechanisms. Shrinkage porosity forms during solidification due to the volumetric contraction associated with the liquid-to-solid transformation. On the other hand, trapped air, created by turbulent flow and rapid mold filling during HPDC process, is the main source of gas porosity. Lee *et al.*^[11] investigated the effects of gate velocity, intensification pressure, and melt

P. SHARIFI and J.T. WOOD are with Western University, 1151 Richmond Street, London, ON, N6A 3K7, Canada. Contact e-mail: psharif2@uwo.ca J. JAMALI is with American University of the Middle East (AUM), 220 Dasman, 15453, Eqaila, Kuwait. K. SADAYAPPAN is with CanmetMATERIALS, 183 Longwood Rd S, Hamilton, ON, L8P 0A5, Canada.

Manuscript submitted April 5, 2017.

Article published online May 3, 2018

temperature on the area fraction of gas porosity and shrinkage porosity separately for simple magnesium plate casting. They noticed that the gas porosity is affected by intensification pressure, gate velocity and the melt temperature while these parameters don't have a significant effect on shrinkage porosity. They did not measure the amount of defect band and shrinkage porosity separately. They considered the defect band as shrinkage. Although defect band contains less shrinkage porosity in die cast magnesium alloys, but their formation mechanisms are distinctly different and independent from shrinkage porosity.

Dahle *et al.*^[14] proposed a theoretical framework that defect bands are formed by a combination of a fraction solid gradient away from surface layer and the presence of ESGs in the center region as a result of lift forces on the solid. They pointed out that there exists a narrow region of lower fraction solid (fs) between skin and core region, and that deformation will be concentrated in this region which could, then, form defect band. Laukli *et al.*^[15] reported that the position of the defect bands is affected by the die temperature and the fraction of ESGs which are produced by partial solidification of melt in the shot sleeve. They, also, observed that the area fraction of ESGs increases with a decrease in the melt superheat and decreases with an increase in the melt superheat.

Due to various defects are formed by different mechanisms, their dependencies on the process parameters are not the same. Furthermore, most of the previous studies^[9-11,14,15] focused on simple geometries which ignored the contribution of local filling and solidification on the formation of defects. The formation of defects in large, complex castings is influenced by the position due to different molten metal flow characteristics and location in the casting such as Knit line, Last-to-fill, Last-to-solidify, and Close-to-gate.

Due to very high flow and cooling rates in the HPDC process, the quantitative measurement of cooling rate is practically very difficult. Hence, commercial software is suggested to be used to predict the cooling rate in the HPDC process. Many studies^[16-20] have been carried out to predict the filling and solidification using the commercially available software packages. Software packages are capable of simulating the HPDC operation with respect to the mold pressure, molten metal velocity, and molten metal temperature. Simulation software enable researches to identify the local filling and solidification during the casting process.

This study aims to investigate the effects of slow stage of piston velocity, fast stage of piston velocity, intensification pressure, and die temperature on the area fraction of the total defect, shrinkage porosity, gas porosity, defect band, and ESGs in HPDC of magnesium alloy AM60. In this paper, the local filling and

solidification conditions are predicted using the commercial software ProCAST™ as well, to better understand the defect formation mechanism.

II. MODELING METHOD

In this study, the commercial software ProCAST™ was employed to identify the appropriate process parameters before conducting the HPDC experiments. This commercial software is based on finite element to solve thermal and fluid equations in casting systems. In this study, 3D solid models of the component along with the two halves of the dies were created. The 2D and 3D meshes are generated by ProCAST™ automatically. Three-node linear trilateral elements were employed, different mesh densities for the casting and the die were used in an effort to reduce implementation time. In order to conduct the mesh convergence study, the central solidification time was determined from four different mesh size ranges and simulation results were then compared to these mesh size ranges. The element sizes were then utilized for the mesh ranged from 0.2 to 0.5 mm for the casting, and from 7.0 to 14.0 mm for the die sections and cooling channels. Before numerical simulation, CAD model was utilized for the 3D modeling of the casting including the runner, dies, and shot sleeve. In this study, the following assumptions were made to implement the simulation:

1. The gas phase is incompressible.
2. The fluid flow behavior is not shear dependent.
3. Thermodynamic databases are calculating the fraction of solid and enthalpy curves and solidus and liquidus temperatures on the basis of the alloy composition.
4. The initial temperature of the casting is the melt temperature

The thermophysical properties used for simulation are presented in Table I. It should be noted that heat-transfer coefficient is a function of temperature during the simulation process. For all the sets, the interfacial heat-transfer coefficient (IHTC) value of metal/runner and metal/shot sleeve is assigned 8000 and 10,000 Wm⁻² K⁻¹ respectively. Also, a constant value of heat-transfer coefficient was employed for die-die and piston-die interfaces. In this study, the IHTC value is the maximum value of interfacial heat-transfer coefficient between metal and die.

III. EXPERIMENTAL PROCEDURE

The casting experiments were conducted at CanmetMATERIALS laboratory in Hamilton, Canada. The castings were produced using a 1200 tone,

Table I. The Values of Thermo-Physical Variables

Thermo-Physical Variables	T_l (K)	T_s (K)	α (m ² /s)	k (W/m °C)	ρ (kg/m ³)	c (J/kg °C)	L_f (kg/J)
Values	888 [615 (°C)]	838 [565 (°C)]	0.044	101.8	1800	1333.8	370,000

Table II. Chemical Composition of AM60 Alloy

Alloy	Mg	Al	Zn	Mn	Si	Cu	Fe	Ni	Be
AM60	93.6	6.1	—	0.32	0.005	0.001	0.001	0.001	0.001

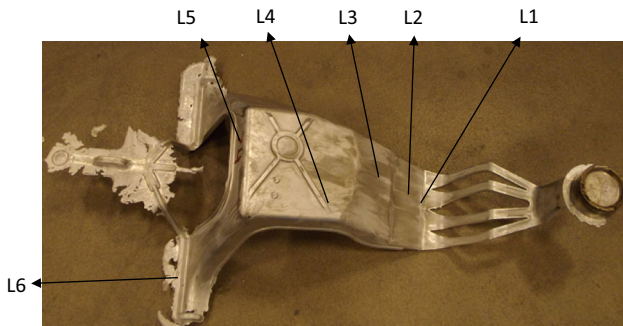


Fig. 1—The shock tower casting with gates and overflow. Selected locations for the characterization are marked from L1 to L6.

cold-chamber die cast machine. The magnesium alloy AM60 composition is shown in Table II. Figure 1 shows the geometry of shock tower and the locations of biscuit, runners, gates, vents, and overflows. Coupons used in the characterization of casting microstructure were obtained from six different locations in shock tower. The shock tower was produced using tools designed to be evacuated during filling to reduce the level of gas porosity. To obtain a quasi-steady-state temperature in the shot sleeve and die, 10 shots were made before producing the investigated casting in this experiment. Six samples of $2 \times 1 \times 3$ mm were extracted from different locations as shown Figure 1. The local solidification condition for each location was identified by simulating the filling and solidification processes. The shock tower has been produced by different sets of process parameters as indicated in Table III. Three castings for each set of process parameters were chosen and examined.

A. Metallography

Sample preparation for microstructural examination was carried out by wet grinding with progressively finer grades of sandpapers from 180 to 1200. The samples were further polished with a polishing cloth in slurries of $1 \mu\text{m}$, and finally $0.5 \mu\text{m}$ diameter alumina in water and ethanol on an automatic polisher. The applied force was 10 N, and a polishing speed of 15 to 20 rpm was selected. After polishing, the specimen is thoroughly washed with ethanol and ultrasonically cleaned. Optical microscope and digital image analysis (DIA) software were then used to measure the area fraction of porosity.

B. Measurement of Area Fraction of ESGs

The grain structure was etched by a solution containing 5 pct citric acid. Optical microscope and digital image analysis software were then used to measure the

grain area fraction of ESGs. The measurement of area fraction of ESGs was performed using image analysis software Clemex. In order to measure area fraction of ESGs in the cross section of casting, the image montages have been made by eight contiguous fields. The variations of ESGs were examined both in transverse and longitudinal directions. The binary operation in the image analysis software enables users to detect the interested area. The grains are detected using binary feature of the image analysis software.

C. Measurement of Area Fraction of Different Defects

The total area fraction of gas porosity, shrinkage porosity were determined by taking an average for 15 individual frames on each specimen, at a magnification of $\times 100$. In this study, gas porosity has been separated from shrinkage porosity based on their shape differences. The gas porosities are assumed to mostly have round shape in 2D image while shrinkage porosities have a thin long crack-like appearance. Figure 2 shows the procedure which is applied to differentiate between the gas and shrinkage porosities. First, the image is converted into its binary image by thresholding as shown in Figure 2(b). Second, the gas porosities with a diameter larger than $20 \mu\text{m}$ are separated from the field of view as shown in Figure 2(c). Third, the separation of small gas porosity from shrinkage porosity was accomplished using the differences in roundness factor. The following equation is the basic definition of roundness factor in image analyses software.

$$\text{Roundness Factor} = \frac{4 \times \text{Area}}{\pi \times L^2} \quad [1]$$

where L is the longest diameter, and the roundness is equal to 1 for a perfect circular object. In this study, the roundness factor of gas porosity is considered from 0.5 to 1. Thus, the shrinkage porosity is separated from gas porosity as shown in Figure 2(d). Finally, the total area fraction of porosity is calculated by adding area fraction of small gas pores with area fraction of big ones.

In order to measure area fraction of defect bands, the images from 12 contiguous fields were montaged as shown in Figure 3. The montaged image is converted into its binary image by thresholding (Figure 3(b)) and separating defect bands from shrinkage and gas porosities (Figure 3(c)). Finally, the area fraction of defect band is measured using image analysis software. It should be noted that in the samples containing defect band, the area fractions of gas porosity and shrinkage porosity are measured separately using the mentioned method. In this study, the total area fraction of porosity contains area fractions of gas, shrinkage, and defect bands.

Table III. The Different Sets of Process Parameters

Process Parameters	Slow Speed of Piston (m/s)	Fast Speed of Piston (m/s)	Intensification Pressure (bar)	Die Temperature (°C)
A	0.9	5	600	160
B	0.7	5	600	160
C	0.9	3	600	160
D	0.9	5	400	160
E	0.9	5	600	240

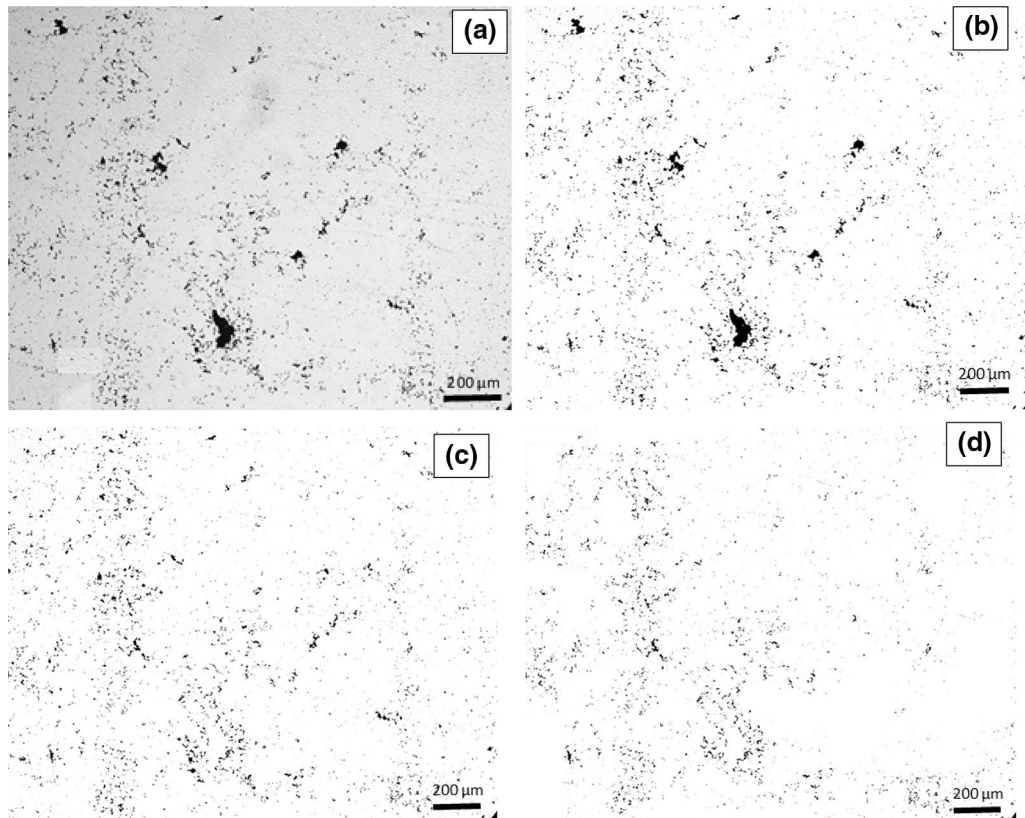


Fig. 2—Separation of gas porosity from shrinkage (a) Gray scale of typical micro structure magnesium alloy AM60 including gas porosity. (b) Binary image of the gray scale image. (c) Small gas pores and shrinkage porosity. (d) Shrinkage porosity.

IV. RESULTS

Figure 4 presents a typical polished section of each location. Figure 5 shows the variation in area fraction of total porosity, shrinkage porosity, gas porosity and defect band for each location. These data enable investigating the effects of process parameters on different kinds of porosity. A filling and solidification simulation was performed using Procast to characterize the general solidification conditions for shock tower as shown in Figure 6. The local solidification conditions for each of the sampling locations were identified such as knit-line region, last-to-solidify region, and last-to-fill region. As shown in Figure 6, Sample 1 is located inside a knit-line region where two molten metal flows meet. Practically, the knit line might occur in Location 2 or 3. Simulation results indicate that Location 4 and Location 6 are last-to-solidify regions and last-to-fill region,

respectively. Last-to-solidify regions are generally the thicker parts of the casting such as Location 4. As seen in Figure 4, large gas porosity was found in the Location 4. The total area fraction of porosity in Location 4 is much higher than other locations as shown in Figure 5. The diameters of some gas porosities exceed 500 μm in the Location 4. The formation of large gas pores is due to the fact that molten metal remains in the liquid state for longer periods of time in the last-to-solidify regions and solidification occurs without sufficient molten metal. Mold-filling simulations indicate that the flow does not continue after passing Location 5 because there is no overflow in front of this location. This induces accumulation of gas porosity in Location 5. The last-to-fill location is typically farthest away from the gate and last-to-receive molten flow, such as Location 6. As seen in the figure, the defect band was observed just in Locations 5 and 6. No defect band was

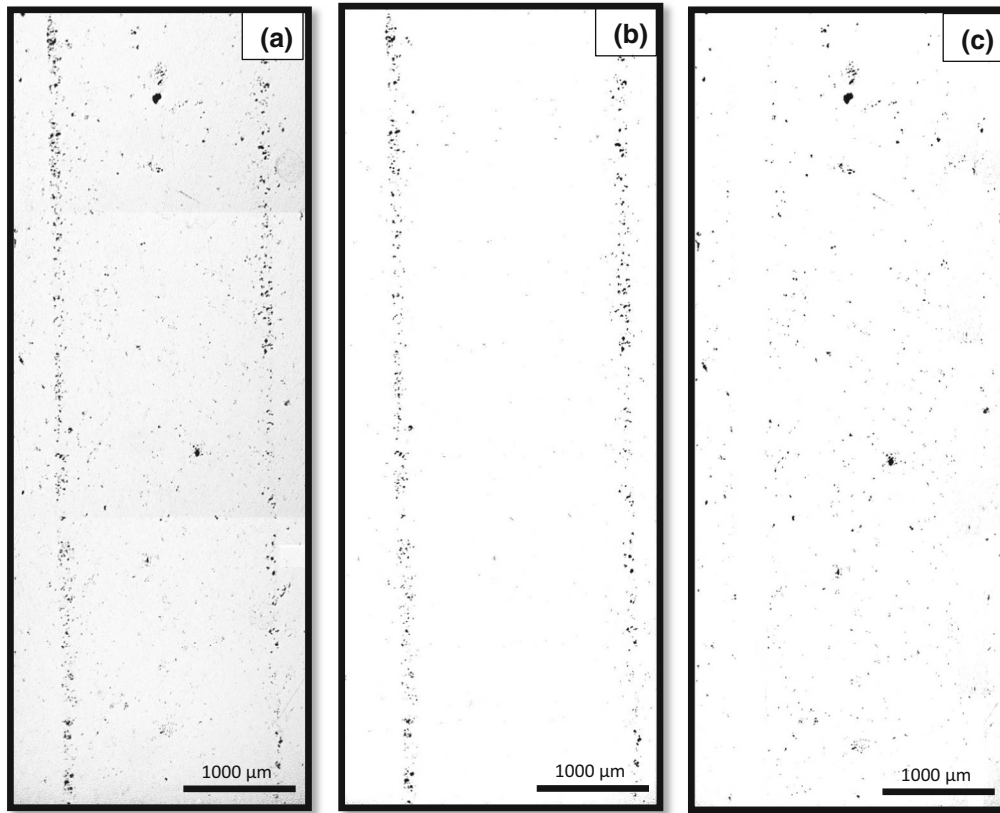


Fig. 3—Separation of defect band from gas and shrinkage porosities (a) gray scale of 12 montaged pictures of microstructure from Location 6 (b) defect band (c) shrinkage and gas porosities.

observed in Locations 1 through 4 for all sets of process parameters.

Figure 5 presents the optical micrograph of the etched microstructure of each location. Figure 8 shows the variations in ESGs for various locations with different sets. As can be seen in Figure 7, locations near the gate (Location 1 and Location 2) include significantly larger fractions of ESGs, whereas this microstructural feature is more dilute in the position farther away from the gate. In both locations, the grain structure at the center consists of coarse grains surrounded by small grains, and nearer the surface, fewer coarse grains are observed in these positions. In other locations, the entire skin region contains refined grains, while in the core region, some ESGs can be observed. This morphology of grains formed in the shot sleeve prior to inserting the molten material to the die cavity and its migration to the center as a result of lift forces that acted on the solid. The ESG is characterized by the dendrites and fragmented dendrites ranging from 15 to 80 μm and an average length of 43 μm .

In order to study the influence of the slow stage of piston velocity on the amount of porosity, the shock tower has been produced with Set A and Set B including the same values of all process parameters except the slow stage of piston velocity. As seen in Figure 7, there is no relationship between the amounts of the different

classes of porosity and the slow stage of piston velocity. In order to investigate the influence of fast stage of velocity, Sets A and Set C were applied using the same process parameters except the fast stage of piston velocity. As shown in Figure 7, the fast stage of piston velocity has an effect on the variation of area fraction of gas porosity.

Intensification pressure effects can be seen in the comparison of Set A and Set D. As seen in Figure 7, intensification pressure influences on the total area fraction of porosity, shrinkage porosity, gas porosity, and defect band. The influence of die temperature on the amount of porosity can be characterized by making comparison between the results of Set A and the results of Set E. As shown in Figure 7, the die temperature shows significant effects on the total area fraction of defect for Locations 5 and 6, while die temperature has negligible effect on the area fractions of total amount of porosity, shrinkage porosity, and gas porosity for other locations. As shown in Figure 8, the area fraction of ESGs shows a significant reduction from locations near the gate to the farther locations regardless of which set of process parameters was applied. As shown in Figure 8, while the amount of ESGs is not affected by the intensification pressure, it is dependent on the slow and fast stages of piston velocity and die temperature for locations near the gate.

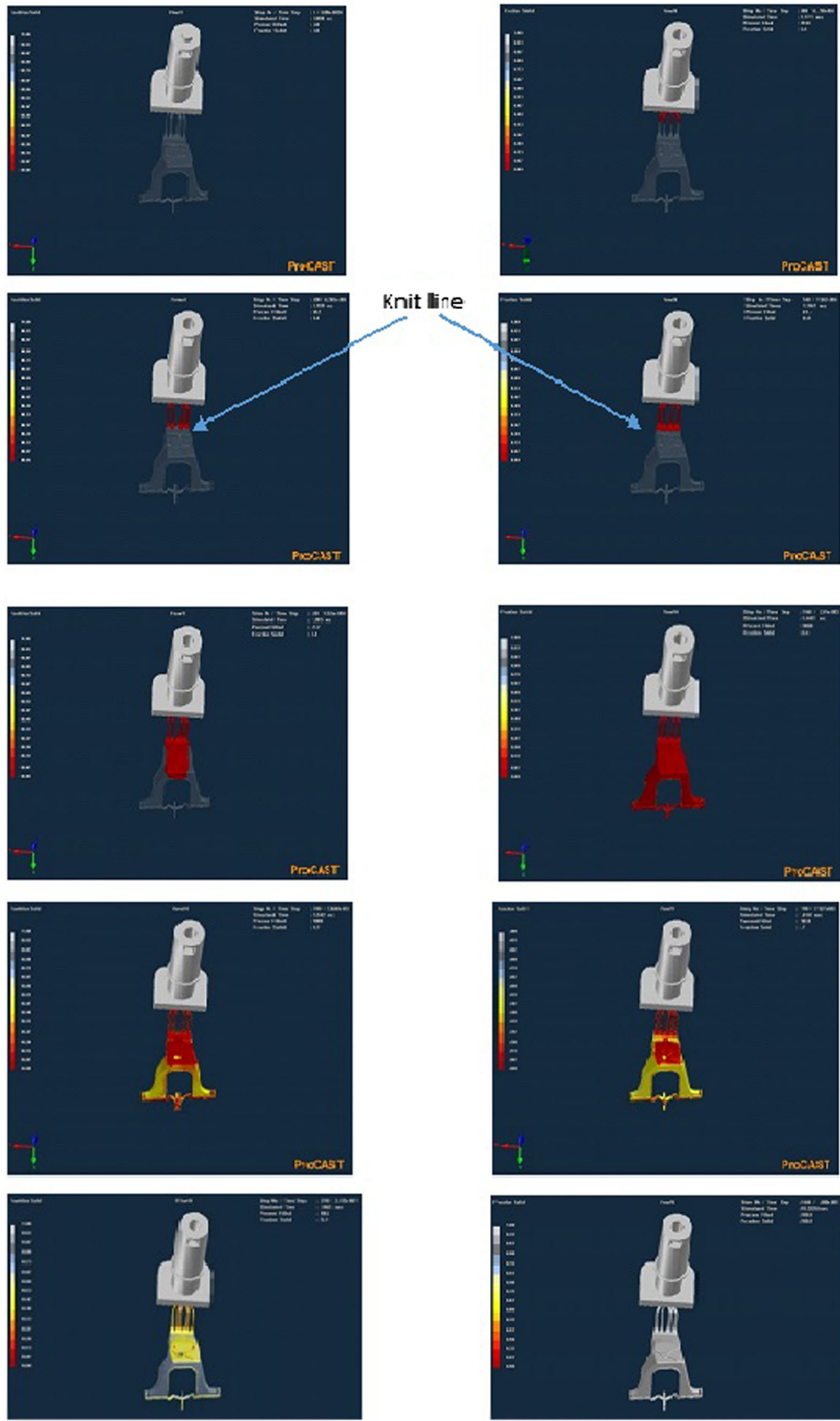


Fig. 4—Filling sequence and solidification conditions predicted in Pro-cast. Arrows show the location of knit lines.

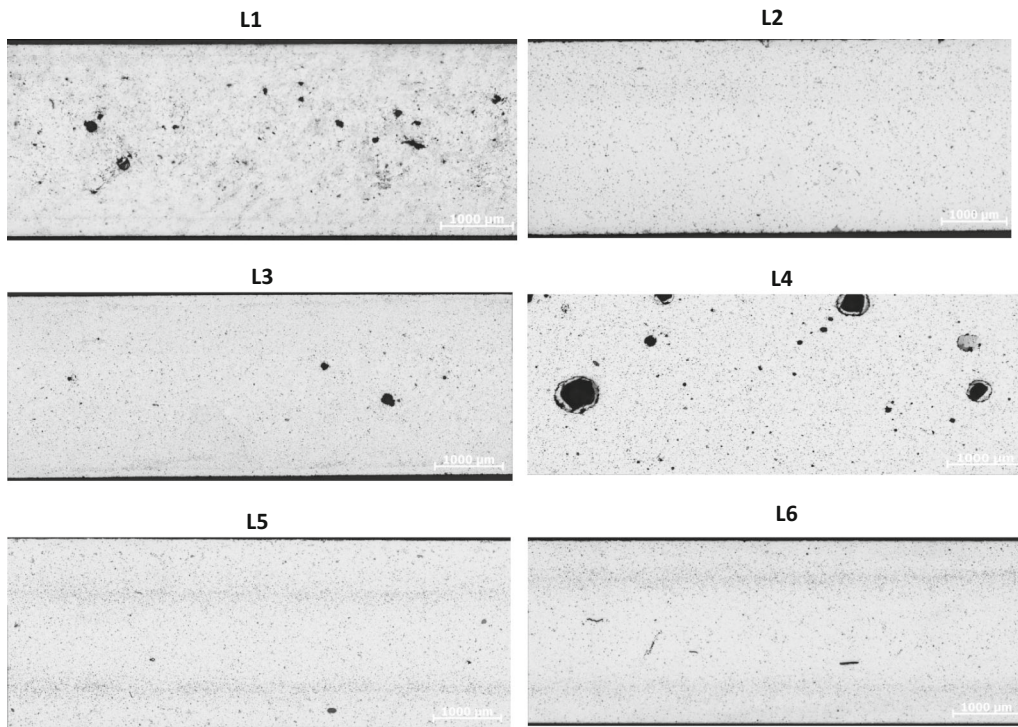


Fig. 5—The montage of micrographs covering the thickness of sample cut from Locations 1 to 6.

V. DISCUSSION

As shown in Figure 7, there is no significant difference between the application of Set A and Set B in the amount of total porosity, shrinkage porosity, and gas porosity. Therefore, these porosities do not show any dependency on the slow stage of piston velocity. The primary purpose of the slow stage of piston velocity (V1) is to build up a wave that forces the air to the front and to prevent entrapment of air during the flow. If the slow stage of piston velocity exceeds an optimal value, it may cause a breaking wave, resulting in the entrapment of air. For this reason, we avoid using considerable variation between Set A and Set B in the slow stage of piston velocity level. However, the area fractions of porosity were not affected by the slow stage of piston velocity, while a significant reduction in the area fraction of ESGs is found by increasing the slow stage of piston velocity for locations near the gate. It is due to the reduction in the contact time between the liquid metal and shot sleeve wall.

A comparison of the results between Set A and Set C indicates that the reduction in the fast stage of piston velocity leads to a reduction in the total area fraction of porosity for all locations. The fast stage of piston velocity (V2) aims to complete filling the cavity of die casting. As can be seen in Figure 7, the amount of gas porosity in Set C is lower than the percentage of gas porosity in Set A for all locations. This is due to the reduction of turbulent flow caused by a lower level of the fast stage of piston velocity. Obviously, higher turbulent flow during filling cavity leads to more air in

the liquid melt. The fast stage of piston velocity does not show the same impact on shrinkage porosity for all locations. In Locations 1, 2, and 4, the amount of shrinkage increases with the increasing fast stage of piston velocity, while the percentage of shrinkage decreases in other locations with the increasing fast stage of piston velocity. These differences mean that fast stage of piston velocity results in various formations of shrinkage in different locations of the cast. More studies are necessary to understand the reasons for these differences.

The fast stage of piston velocity has more influence on the amount of gas porosity in locations close to the gate compared with the other locations. Higher fast stage of piston velocity increases the average percentage of gas porosity by approximately 45 pct in Location 1, whereas it has a smaller effect in increasing the gas porosity to approximately 12 pct in Location 6. In fact, the average percentage of gas porosity is raised by knit-line condition occurring in locations near the gate as shown in Figure 4. These locations are expected to have higher amounts of porosity, due to entrapped gas and oxide inclusion when two liquid fronts meet. This finding shows that the area fraction of gas porosity in locations at knit-line region is more sensitive to fast stage of piston velocity than the area fraction of porosity in other locations. Figure 7 indicates that the percentages of the total porosity and gas porosity in the Location 1 are much higher than those in Locations 2 and 3 when the same process parameters were used. This suggests that the knit line probably occurred at Location 1 for all sets of process parameters.

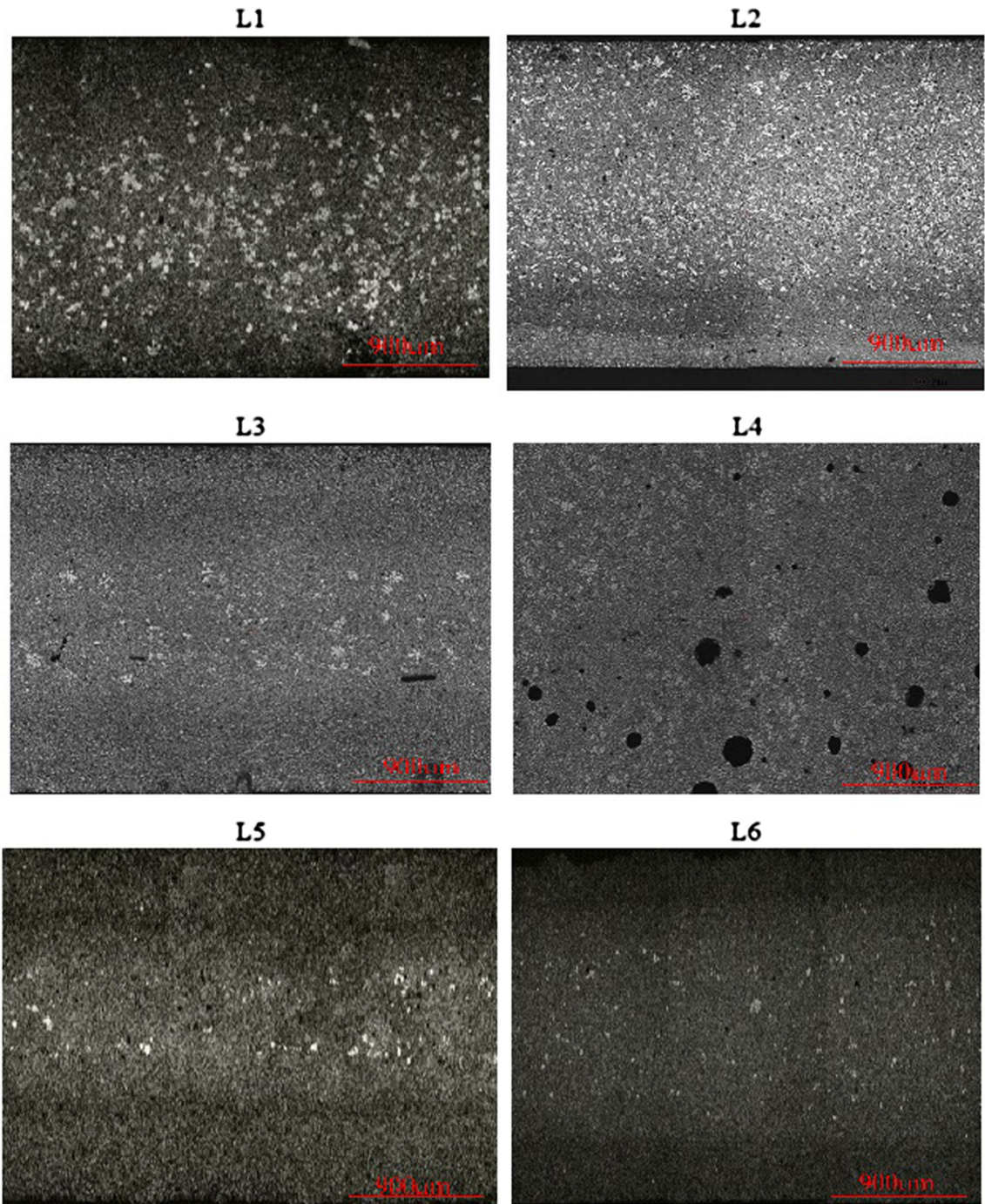


Fig. 6—The typical microstructure of six locations.

The purpose of intensification pressure (IP) is to compress any entrapped gas and transfer further material into the die cavity to feed the shrinkage of the casting during solidification. As shown in Figure 7, the intensification pressure has a very low effect on the amount of shrinkage porosity compared with the gas porosity. The area fraction of gas porosity is remarkably decreased by higher level of intensification pressure. The application of intensification pressure has more influence on the reduction of gas porosity level in Location 4

compared with other locations. This is because there is a very large pore formed in the last-to-solidify region, and the higher level of intensification pressure reduces the size and the number of gas pores. The average size of gas porosity is decreased from 312 to 195 μm when the intensification pressure is increased from 400 bar to 600 bar, respectively. The significant reduction in the area fraction of porosity in Location 4 is attributed to the compression of the gas porosity when a higher level of intensification pressure is applied.

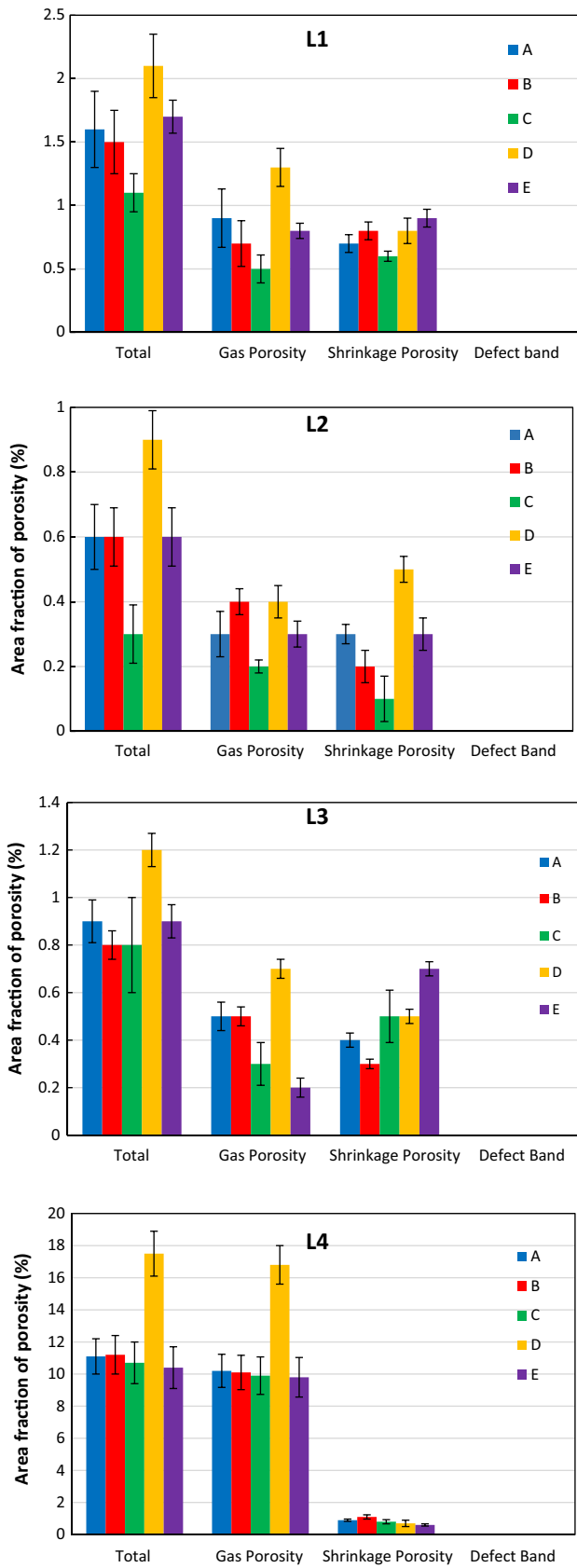


Fig. 7—The effects of different sets of process parameters on the amounts of various porosities at different locations. The error bars represent one standard deviation resulting from three samples for each set of process parameters.

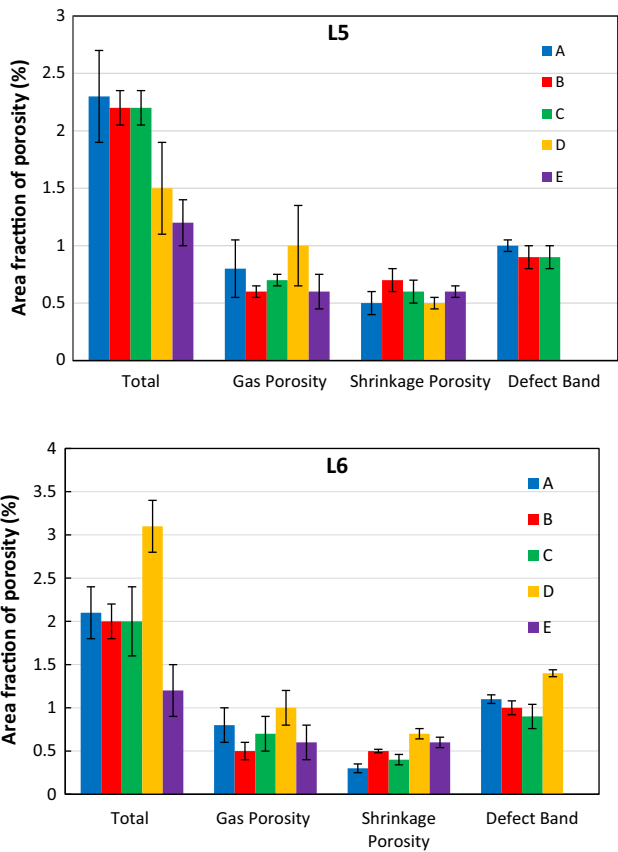


Fig. 7—continued.

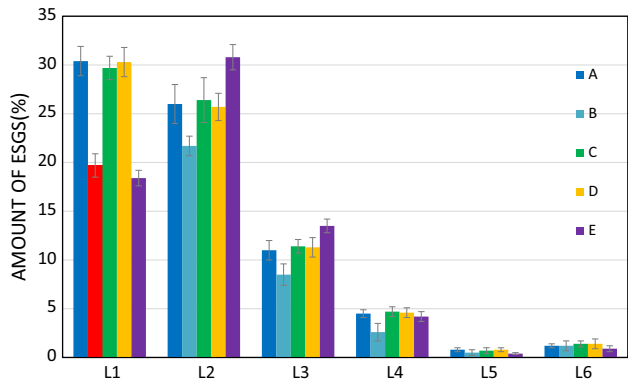


Fig. 8—The process parameters effects on the amounts of ESGs for different locations.

The effect of intensification pressure on the total area fraction of porosity alters from location to location. As can be seen in Figure 7, a higher level of intensification pressure reduces the total area fraction of porosity for all locations except Location 5. This is attributed to the disappearance of a defect band in Location 5 when lower level of intensification pressure is used, resulting in the reduction of the total area fraction of porosity. In addition, the defect band is observed for the Sets A, B, and C at Locations 5, when the higher level of

intensification pressure was applied. This can be explained by higher local deformation occurring in the locations closed to overflow region when higher intensification pressure is applied. There is a narrow region of lower fraction solid between skin and core region, and that the deformation is concentrated in this region, which could then form defect band. Since the cavity is filled before applying intensification pressure, the skin region forms before applying intensification pressure. Therefore, there is a significant gradient of solid fraction between skin region and core region before applying intensification pressure. The defect band probably forms in the last stage of solidification, whereas solid fraction is very high and the applied local pressure is sufficient. Regarding defect band formation, some researchers^[2,14] believed that there is direct relationship between defect band and ESGs. In this study, it was observed that defect band forms in the locations with the lowest amount of ESGs, as a result, there is no relationship between ESGs and defect band. The same observation was reported by Gourlay^[16] who reported defect band might form in the few or absence of ESGs.

As shown in Figure 7 defect band has a considerable share to increase the total area fraction of porosity in the Locations 5 and 6. Previous researchers^[9-11] generally believed that the application of intensification pressure in the HPDC process lead to reduces the total amount of porosity. Most of the studies focused only on the simple geometry that ignores the local effect of intensification pressure on the defect band formation. In this study, we found that the application of higher intensification pressure lead to the significant reduction in the amount of gas porosity, but increasing the intensification pressure might increase the total area fraction of porosity *via* defect band formation in some locations of complex geometry component.

As seen in Figure 7, the effect of die temperature variation on the total area fraction of porosity is more sensitive to Locations 5 and 6 compared with other locations. These data appear to indicate the trend of a decrease in the total amount of porosity with the increasing die temperatures for Locations 5 and 6. It is due to the defect band which disappeared when the die temperature is increased from 160 °C to 240 °C. In addition, the defect band was observed in the Location 6 for all sets except the Set E, where a higher level of die temperature was used, presumably reducing the solid fraction in the casting at the time of Intensification Pressure application. These observations are consistent with the findings of Gourlay^[21,22] who observed that defect bands disappeared with the increasing die temperature.

As shown in Figure 8, the position of ESGs is more sensitive to die temperature compared with other process parameters. The area fraction of ESGs in Location 2 is much higher than the area fraction of ESGs in Location 1 when the Set E was applied. In addition, area fractions of ESGs shows that the highest value in Location 2 and the lowest value in Location 1

occur in the Set E compared with the other sets (*i.e.*, Set A through Set E). This variation can be explained by the increasing fluidity of liquid metal, whereas the die temperature increases during filling cavity, because less solidification occurs near to the die wall. As a result, more ESGs transfer further from the locations near the gate to other locations.

It was observed that at Location 1 through Location 4, the total area fraction of porosity *via* the Set C is significantly less than the total area fraction of porosity in the same locations with the other sets. Also, the percentages of total area fraction of porosity in Locations 5 and 6 using the Set E are smaller compared with the other sets applied. As discussed, the effects of process parameters on the amount of shrinkage porosity, gas porosity, and defect band were found to be varying from location to location. These findings confirm that the local solidification and filling conditions, similar to process parameters, play a major role in the formation of different kinds of defects.

VI. CONCLUSION

In this study, metal flow, filling, and solidification of a shock-tower die casting were studied by simulating the process using commercial software ProCAST™. The simulation was used to identify various local solidification features such as knit line, last-to-solidify, and last-to-fill regions. In this study, the effects of four process parameters (slow stage of piston velocity, fast stage of piston velocity, intensification pressure, and die temperature) on the variations of different kinds of defects such as shrinkage porosity, gas porosity, defect band, and ESGs were investigated.

It was observed that the area fraction of ESGs only depends on the residence time in the shot sleeve, and is, therefore, controlled by the slow stage of piston velocity. The percentage of gas porosity is affected by the fast stage of the piston velocity (affecting air entrapment) and intensification pressure (affecting the pressure balance at the void-metal interface). It was found that the area fraction of gas porosity at the knit-line region is more sensitive to the fast stage of the piston velocity than the area fraction of porosity in other locations.

The formation of the defect band is dependent upon the local solid fraction at the time the intensification pressure is applied and is, therefore, affected by the magnitudes of the intensification pressure and the die temperature (controlling local solidification conditions). It was observed that the application of higher intensification pressure significantly reduced the amount of gas porosity, but it might increase the total area fraction of porosity *via* defect band formations in some locations of complex geometry component. These observations showed the major significant roles that the local solidification and filling conditions play in the formation of different kinds of defects.

ACKNOWLEDGMENTS

The work is jointly supported by NSERC–Automotive Partnership Canada program and NRCan’s Office of Energy R&D through the Program on Energy R&D. Technical support from the Magnesium Front End R&D (MFERD) research team at USAMP is appreciated. The authors of this paper would also like to thank G. Birsan and F. Benkel of the casting group at Canmet MATERIALS for their assistance in performing casting trials.

REFERENCES

1. B.L. Mordike and T. Elbert: *Mater. Sci. Eng. A.*, 2001, vol. 302, pp. 37–45.
2. A.K. Dahl, S. Sannes, D.H. St. and H. Westengen. John: *J. Light Metals*, 2001, vol. 1, pp. 99–103.
3. Z. Yang, A. Maurey, J. Kang, and D. Wilkinson: *J. Mater. Charact.*, 2016, vol. 114, pp. 254–62.
4. A. Balasundaram and A.M. Gokhale: *Mater. Charact.*, 2001, vol. 44, pp. 419–26.
5. S. Amira, D. Dubé, R. Tremblay, and E. Ghali: *Mater. Charact.*, 2013, vol. 76, pp. 48–54.
6. P. Sharifi, Y. Fan, J.P. Weiler, and J.T. Wood: *J. Alloys Compd.*, 2014, vol. 605, pp. 237–43.
7. P. Sharifi, Y. Fan, H.B. Anaraki, A. Banerjee, K. Sadayappan, and J.T. Wood: *Metall. Mater. Trans. A.*, 2016, vol. 47A, pp. 5159–68.
8. J.P. Weiler, J.T. Wood, R.J. Klassen, E. Maire, R. Berkmortel, and G. Wang: *J. Mater. Sci.*, 2005, vol. 395, pp. 315–22.
9. M.S. Dargusch, G. Dour, N. Schauer, C.M. Dinnis, and G. Savage: *J. Mater. Process. Technol.*, 2006, vol. 180, pp. 37–43.
10. Y.J. Huang, B.H. Hu, I. Pinwill, W. Zhou, and D.M.R. Taplin: *Mater. Manuf. Processes.*, 2000, vol. 15, pp. 97–105.
11. S.G. Lee, A.M. Gokhale, G.R. Patel, and M. Evans: *Mater. Sci. Eng. A.*, 2006, vol. 427, pp. 99–111.
12. J.P. Weiler and J.T. Wood: *J. Alloys Compd.*, 2012, vol. 537, pp. 133–40.
13. C.D. Lee, T. So, and K.S. Shin: *Mater. Sci. Eng. A.*, 2014, vol. 599, pp. 28–37.
14. A.K. Dahle and D.H. StJohn: *Acta Mat.*, 1999, vol. 47, pp. 31–41.
15. H.I. Laukli, O. Lohne, S. Sannes, H. Gjestland, and L. Arnberg: *Int. J. Cast Metals Res.*, 2016, vol. 16, pp. 515–21.
16. P. Sharifi, Y. Fan, K. Sadayappan, G. Birsan, J.T. Wood: *Magnesium Technology 2015*, TMS, Warrendale, PA, 2015, pp. 351–56.
17. P. Sharifi, J. Jamali, K. Sadayappan, and J.T. Wood: *J. Mater. Sci. Technol.*, 2018, vol. 34, pp. 324–34.
18. J. Song, S.M. Xiong, M. Li, and J. Allison: *Mater. Sci. Eng. A.*, 2009, vol. 520, pp. 197–201.
19. C. Dørum, H.I. Laukli, and O.S. Hopperstad: *Comput. Mater. Sci.*, 2009, vol. 46, pp. 100–11.
20. P. Sharifi, Y. Fan, G. Birsan, and J. Wood: *Mater. Sci. Forum.*, 2017, vol. 879, pp. 1755–59.
21. C.M. Gourlay, H.I. Laukli, and A.K. Dahle: *Metall. Mater. Trans. A.*, 2008, vol. 38A, pp. 1833–44.
22. C.M. Gourlay, H.I. Laukli, and A.K. Dahle: *Metall. Mater. Trans. A.*, 2004, vol. 35A, pp. 2881–91.